

We are IntechOpen, the world's leading publisher of Open Access books Built by scientists, for scientists

6,700

Open access books available

180,000

International authors and editors

195M

Downloads

Our authors are among the

154

Countries delivered to

TOP 1%

most cited scientists

12.2%

Contributors from top 500 universities



WEB OF SCIENCE™

Selection of our books indexed in the Book Citation Index
in Web of Science™ Core Collection (BKCI)

Interested in publishing with us?
Contact book.department@intechopen.com

Numbers displayed above are based on latest data collected.
For more information visit www.intechopen.com



Chapter

Electrodeposition of Metal Chalcogenide Thin Films

*Arelis Ledesma Juárez, Alejandro Altamirano Gutiérrez
and Arturo Fernández Madrigal*

Abstract

Chalcogenide metals are compounds with optoelectronic characteristics that allow the construction of various optical and optoelectronic devices. The traditional preparation methods have been techniques such as reactive evaporation and sputtering. However, such methods have limited the construction of devices in large areas, particularly solar cells. Thin film solar cells based on Cu(In, Ga)Se_2 (CIGSe) absorbers have suitable optoelectronic properties. However, their commercial development is scarce since the efficiencies achieved on large surfaces differ from those obtained at the laboratory level. The electrodeposition technique is the most attractive from an economic point of view; however, high conversion efficiencies still need to be achieved with the latter. Several authors attribute this difference to different causes, such as using chemical additives in the preparation. The influence of the salt during its synthesis is not studied, so this work aims to use three different types of metal salts and voltages to produce (CIGSe) absorbing thin films by the electrodeposition technique. Also, the effect of nucleation type on two other substrates is studied. The various features of structural, morphological, atomic composition, and electrochemical characterization were to understand the formation, growth, and morphology of CIGS films, to obtain a suitable stoichiometry of thin film solar cells using this absorber.

Keywords: electrodeposition, solar cells, CIGS absorber

1. Introduction

Chalcogenide metals are materials composed of a chalcogen anion with a more electropositive element. They have been formed by those compounds based on sulfides, selenides, and tellurides. These materials contain various metallic minerals and can be used for many applications. Thin films of metal chalcogenide semiconductors find applications such as photovoltaics, batteries, electrocatalysis, or photonics. Examples of ternary chalcopyrite semiconductor materials such as CuZnSn(S, Se)_2 (CZT(S, Se) [1], CuInS_2 , CuIn(S, Se)_2), or Cu(In, Ga)Se_2 (CIGSe) are among the most promising thin film materials for solar cell applications due to their properties and long-term stability, as well as adequate performance in low-light conditions [2], and suitable bandgap and absorption coefficient values [1, 3, 4]. Solar cells based on CIGSe

films are the ones that have achieved high efficiencies, on the order of 23.35% using vacuum methods and 17.5% by the electrodeposition technique.

The electrodeposition technique is the most promising for preparing low-cost semiconductor solutions [5–7] and has been used to develop CdTe thin-film photovoltaic modules [8]. This technique employs the electro-reduction of ions to a specific reduction potential on a substrate to form thin films by applying an electric field. During this process, many parameters are involved, which influence the formation of a crystalline structure that allows achieving adequate growth of the thin film to form solar cells. Among the main parameters contributing to this type of film are the solution's pH, the deposition temperature, the additives added to the electrolytic baths, the position of the electrodes, the type of metallic salts used, the types of complexing agents, etc. These parameters mainly affect the type of nucleation, crystal size, electrical, optical, and optoelectronic properties, etc. For example, polyamide substrates treated with potassium fluoride as substrate obtained a cell with an efficiency of 20.4% [9]. Doping with rubidium fluoride (RBF) or cesium fluoride (CsF) improves the efficiency of solar cells by up to 20% [10]. Power has also increased by using Zn(O, S)-based window layers by 21% efficiency [11]. The addition of buffer solutions such as sodium sulfamate and potassium bi-phthalate helps stabilize the solution's pH, allowing Ga and ions to be incorporated into the films [12]. Using complexing agents has been an important strategy; thus, using KCN or potassium sodium potassium tartrate has allowed the control of Ga and ions into the films [13–15]. Some treatments applied to the coatings, through hydrogen and selenium, have increased efficiency by 9.4% [1]. It is essential to mention that incorporating In and Ga in the film is a determining factor in obtaining a film with an adequate structure, which allows the formation of solar cells with high conversion efficiencies. In this sense, this work describes the characteristics of CIGSe thin films using three types of metallic salts to prepare the electrolytic bath.

2. Experimental section

2.1 Materials and equipment

The co-electrodeposition technique uses three different salts to prepare the CIGSe thin films. **Table 1** shows the molar concentration of each metal salt used in the preparation of each bath. The purity and brand of each of the salts are copper (II) chloride dihydrate (99.99%), indium (III) chloride (99.999%), anhydrous gallium (III) chloride (99.99%), lithium chloride ($\geq 99\%$), copper (II) nitrate hydrate (99.999%), indium (III) nitrate hydrate (99.999%), gallium (III) nitrate hydrate (99.9%), lithium nitrate (99.99%), copper (II) sulfate ($\geq 99\%$), indium (III) sulfate hydrate (99.99%), gallium (III) sulfate (99.99%), selenious acid (99.999%). The

Bath No.	2.6 (mM)	4.5 (mM)	10 (mM)	8 (mM)	1 (mM)
1	CuCl ₂	InCl ₃	GaCl ₃	H ₂ SeO ₃	LiCl
2	Cu(NO ₃) ₂	In(NO ₃) ₃	Ga(NO ₃) ₃	H ₂ SeO ₃	LiNO ₃
3	CuSO ₄	In(SO ₄) ₃	Ga ₂ (SO ₄) ₃	H ₂ SeO ₃	Li ₂ SO ₄

Table 1.

The molar composition of each of the salts used in the electrolytic baths.

chemicals were from Aldrich Chemical Co, the reagent lithium sulfate (99.7%), hydrochloric acid 37.4% ACS, nitric acid 70% ACS purchased from Fermont Company, and sulfuric acid 97.4% ACS from J.T. Baker, buffers pH three from Hydrion Company.

Two types of substrates use the first one made on Fluorine Tin Oxide glass, SnO₂:F (FTO) prepared by Delta Technologies. The Mo substrate on glass had designed in-house, using a Balzer BAE 250 direct current sputtering machine, using a Mo target with a diameter of 5.08 cm.

The thin films had prepared using a Bio-Logic SAS potentiostat model VSP s/n:0332 controlled with Ec-lab software. The films were analyzed using X-ray diffraction equipment using the diffractometer model DMAX-2200 with copper K α radiation ($\lambda_{\text{Cu}} = 1.5406 \text{ \AA}$) at 40 kV, and the X-ray beam was at 0.5° grazing incidence (GIXRD). The atomic compositions of the films were obtained by EDS technique using Hitachi microscope model SU1510 SEM, which has a secondary electron detector and an energy-dispersive X-ray detector model INCA-x-act. An electron accelerating voltage of 8 kV and energy emission levels K α for copper, selenium, gallium, and L α for indium have been used to quantify the atomic composition. Atomic composition values were quantified over 600 $\mu\text{m} \times 600 \mu\text{m}$. Micrographs of the films had obtained using a Hitachi model S-5500 SEM microscope with a secondary electron detector. An Alpha-step 100 profilometer has been used for thickness measurement. Diffuse reflectance spectra obtained by UV-VIS measure were performed using a Jasco V-670 spectrophotometer with a 2500-250 nm wavelength range 50 nm.

The absorption spectra had been obtained by the Kubelka-Munk equation [16].

$$\frac{K}{S} = \frac{(1 - R_{\infty})^2}{2R_{\infty}} = F(R_{\infty}) \quad (1)$$

Eq. 1 shows the diffuse reflectance called the Kubelka-Munk function and the absorption coefficient and reflectivity, respectively. S and K are the so-called K-M scattering and absorption coefficients, respectively, and $R_{\infty} = R_{\text{sample}}/R_{\text{standard}}$. The band gap of thin films and the equivalent absorption coefficient had related through the following equation.

$$ahv = A(hv - E_g)^n \quad (2)$$

Eq. 2 [17] α is the linear absorption coefficient, A is an arbitrary constant, $h\nu$ is the photon energy, and n equals 1/2 for direct transition-allowed materials.

When the incident radiation is perfectly diffusely scattered, the absorption coefficient K equals 2α . In this case, the Kubelka-Munk function is proportional to the absorption coefficient α ; we obtain the relation.

$$[F(R_{\infty})hv]^2 = (ahv)^2 \quad (3)$$

The Cyclic voltammetry (CV) and chronoamperometry (C.A.) had done in a three-electrode cell. The working electrode (WE) was FTO or Mo on glass (soda-lime glass) with a Mo film thickness between 1 and 2 microns and an active area of (1 cm \times 3 cm), and the counter electrode (CE) was a platinum grid. Another platinum grid was a reference electrode (REF) for C. Studies, and Ag/AgCl electrode had used as the reference electrode for CV. The deposition potentials for the CIGS films were -0.8 , -0.9 , and 1.0 V . The scan rates were 5 mVs^{-1} , 10 mVs^{-1} , and 20 mVs^{-1} .

3. Results and discussion

3.1 Atomic composition by EDS

Tables 2 and **3** show the atomic composition results obtained by the EDS technique. The number at the end of each sample indicates the applied potential; for example, number 1 corresponds to the application of -1.0 V. For 2 and 3, the applied voltages are -0.9 V and -0.8 V, respectively. **Table 2** shows these results using Mo/glass substrates, and **Table 3** operates $\text{SnO}_2\text{:F}$ (FTO) substrates at three different voltages. The thicknesses achieved for each sample are given in the same tables. The theoretical atomic percentages are Cu, 25%; In, 12.5%; Ga, 12.5%; and Se, 50% [18]; however, it has been found that to build more efficient solar cells, atomic ratios must reach values of 0.93 for $[\text{Cu}]/[\text{In}+\text{Ga}]$ and 0.3 for $[\text{Ga}]/[\text{In}+\text{Ga}]$ [19].

Table 2 shows that the samples obtained with electrolytic baths based on nitrate, sulfate, and chloride $[\text{Cu}]/[\text{In}+\text{Ga}]$ values are high, higher than the desired theoretical value of 0.93. In contrast, the $[\text{Ga}]/[\text{In}+\text{Ga}]$ values are similar to the theoretical value for all samples using the chloride bath and two of the nitrate samples (MN1 and MN2). These results indicate that the Ga content in these samples is adequate, but the Cu content is much higher than desired. This result has repeated for samples FC1, FC2, and FC3, but both values of the atomic ratios had reduced for the samples obtained with nitrate and sulfate baths using the FTO substrate, as shown in **Table 3**.

3.2 X-ray diffraction

Figure 1(a) and **(b)** show the diffractograms of the sample in **Table 1**, using electrolyte solutions of chlorides, nitrates, and sulfates, at potentials of -1.0 , -0.9 , or -0.8 V, respectively, on two different substrates, Mo and FTO. **Figure 1(a)** shows a diffraction peak at $2\theta = 40$, with the assigned plane (110) corresponding to Mo,

Samples	% At.				Thickness (μc)		
	Cu (%)	In (%)	Ga (%)	Se (%)	$\text{Cu}/(\text{In} + \text{Ga})$	$\text{Ga}/(\text{In} + \text{Ga})$	
Mo-Chlorides							
MC1	26.90	15.55	6.10	51.44	1.24	0.28	1
MC2	28.11	15.83	5.48	50.60	1.31	0.25	1
MC3	29.13	12.78	5.39	52.70	1.60	0.29	0.9
Mo-Nitrates							
MN1	40.82	7.71	3.11	48.36	3.77	0.29	0.7
MN2	38.82	9.81	3.96	47.40	2.81	0.30	1
MN3	20.77	30.2	1.43	47.60	0.65	0.04	1
Mo-Sulfates							
MS1	27.18	22.86	1.26	48.7	1.03	0.04	1.1
MS2	42.20	12.67	0.74	44.13	3.14	0.05	2.4
MS3	41.56	14.03	1.38	43.03	2.76	0.07	1.7

Table 2.

Values of atomic percentages and composition ratios of $\text{Ga}/(\text{In}+\text{Ga})$ and $\text{Cu}/(\text{In}+\text{Ga})$, obtained by EDS of CIGS films, using Mo as substrate.

Sample	% At.						Thickness (μc)
	Cu (%)	In (%)	Ga (%)	Se (%)	Cu/(In + Ga)	Ga/(In + Ga)	
FTO-Chloruros							
FC1	26.16	14.46	6.14	53.22	1.27	0.30	0.7
FC2	38.40	7.23	4.78	49.59	3.24	0.39	1
FC3	31.07	11.97	5.01	51.86	1.82	0.30	0.9
FTO-Nitrates							
FN1	17.53	17.34	2.60	62.29	0.88	0.13	0.8
FN2	13.40	23.12	2.20	61.30	0.53	0.09	0.9
FN3	14.64	17.07	3.56	64.73	0.71	0.17	0.8
FTO-Sulfates							
FS1	17.11	32.36	0.49	50.78	0.53	0.01	0.8
FS2	24.69	29.93	3.29	42.10	0.74	0.09	0.7
FS3	23.69	25.81	1.12	49.39	0.88	0.04	0.7

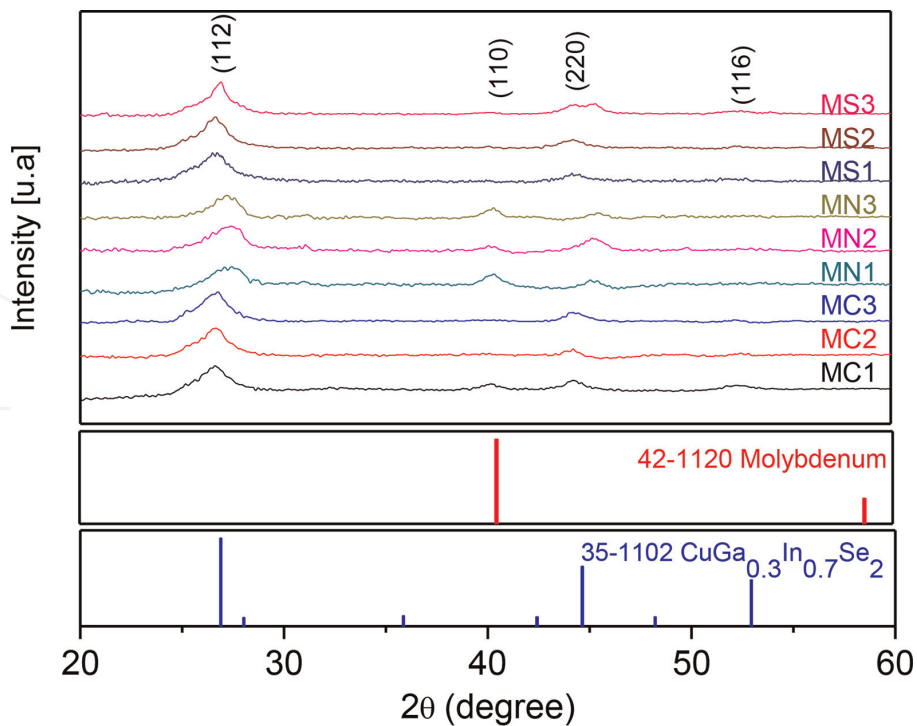
Table 3. Atomic composition percentages and Ga/(In+Ga) and Cu/(In+Ga) composition ratios obtained by EDS of CIGS films using FTO as substrate.

which has a cubic structure with lattice parameters, and whose lattice parameters are $a = b = c = 3.1472 \text{ \AA}$, according to PDF#42–1120. However, in **Figure 1(b)**, no diffraction peak related to the substrate type is observed because the X-ray beam scanning has been performed at a low angle, showing the diffraction planes of the film. **Figures 1(a)** and **1(b)** show that most of the samples have three principal planes identified: planes (112), (220), and (116), which coincide with the PDF #35–1102 structure and correspond to $\text{CuGa}_{0.3}\text{In}_{0.7}\text{Se}_2$. The above planes are practically the same for all samples prepared on Mo and FTO substrate, regardless of the type of electrolytic bath.

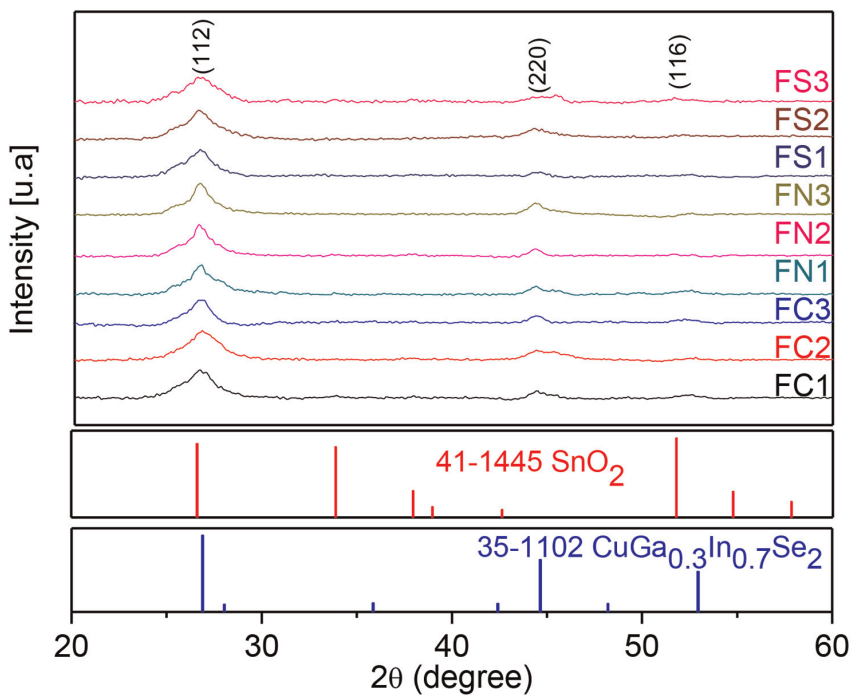
The crystal sizes for the samples shown in **Table 4** had been obtained from the Scherrer equation [20, 21]. **Table 4** shows that the values range from 4 to 15 nm. However, no increase or decrease in their values is observed with different voltages or the type of electrolytic bath.

3.3 Scanning electron microscopy

Figures 2(a,b) shows the morphology of CIGS samples obtained by scanning electron microscopy (SEM) technique, prepared on Mo and FTO substrates, using three types of metallic salts in the electrolytic bath (chlorides, nitrates, and sulfates), at three different voltages. SEM observed the growth of cauliflower-type formation, and clusters are formed by grains whose sizes vary from 0.05 to 0.2 microns. The dimensions of the grains change according to the type of metal salt used, the voltage applied, and the type of substrate. For example, in **Figure 2(a)**, the morphology of CIGS films on a Mo substrate has been observed. Samples MC1, MC2, and MC3, which had been prepared by applying a voltage of -1.0 , -0.9 , and -0.8 V , respectively, show very similar granular growth in all of them, with values of 0.12, 0.125, and 0.16 microns, the size of these grains increasing as the applied voltage decreases. Similar behavior occurs when nitrate and sulfate salts are used, whereas granular growth



(a)



(b)

Figure 1. (a) Shows the X-ray diffraction spectra of CIGS films deposited on Mo, and (b) shows the X-ray diffraction spectra of CIGS films deposited on FTO.

observes a relatively homogeneous distribution. In particular, MS3 shows the formation of flakes instead of spherical grains, like the rest of the samples. This flake formation indicates the formation of Cu-Se [22].

Mo substrate		FTO substrate	
Sample	Crystal size (nm)	Sample	Crystal size (nm)
MC1	8.08	FC1	9.02
MC2	10.84	FC2	4.61
MC3	7.48	FC3	10.55
MN1	15.68	FN1	9.27
MN2	6.23	FN2	10.67
MN3	10.35	FN3	9.48
MS1	7.61	FS1	9.76
MS2	6.91	FS2	8.37
MS3	6.93	FS3	4.81

Table 4. Crystal size calculated from the Scherrer equation, using the highest intensity plane of each sample and principal planes of each of the sample.

Granular growth is observed in samples MS1 and MS2, which form cauliflower-shaped clusters. The development occurs by the clustering of grains on the surface. **Figure 2(b)** shows the morphology of the CIGS samples on an FTO substrate. These samples have a similar morphology to the samples on a Mo substrate. The average grain size ranges from 0.07 to 0.26 microns. Samples FC1, FC2, and FC3 have smaller grains than samples MC1, MC2, and MC3. Samples are obtained with a nitrate bath present small grains that agglomerate to form larger clusters, as shown by the morphology of samples FN1 and FN3, since FN2 presents the formation of flakes whose dimensions are up to 0.26 microns. Samples FS1, FS2, and FS3, formed by clusters of grains whose average size is between 0.16 and 0.21 microns, also show the formation of voids between these clusters.

3.4 J-t transient

The growth of CIGSe films is directly related to the applied overpotential; that is, the development of these films is by the kinetic mechanism of nuclei growth. Therefore, the nucleation and growth mechanisms during the co-deposition of CIGSe films can be studied using the models of the instantaneous and progressive nucleation equations Scharifker and Hill [23] have proposed. Eqs describe these models (4) and (5), respectively, where i_{max} and t_{max} are the peak current and t corresponds to the peak current in the CTT (Current-Time Transient) growth and nucleation region, respectively.

Progressive nucleation in 3D

$$\left(\frac{i}{i_{max}}\right)^2 = \left(\frac{1.2254}{\frac{t}{t_{max}}}\right) \times \left[1 - \exp\left(-2.3367\left(\frac{t}{t_{max}}\right)^2\right)\right]^2 \quad (4)$$

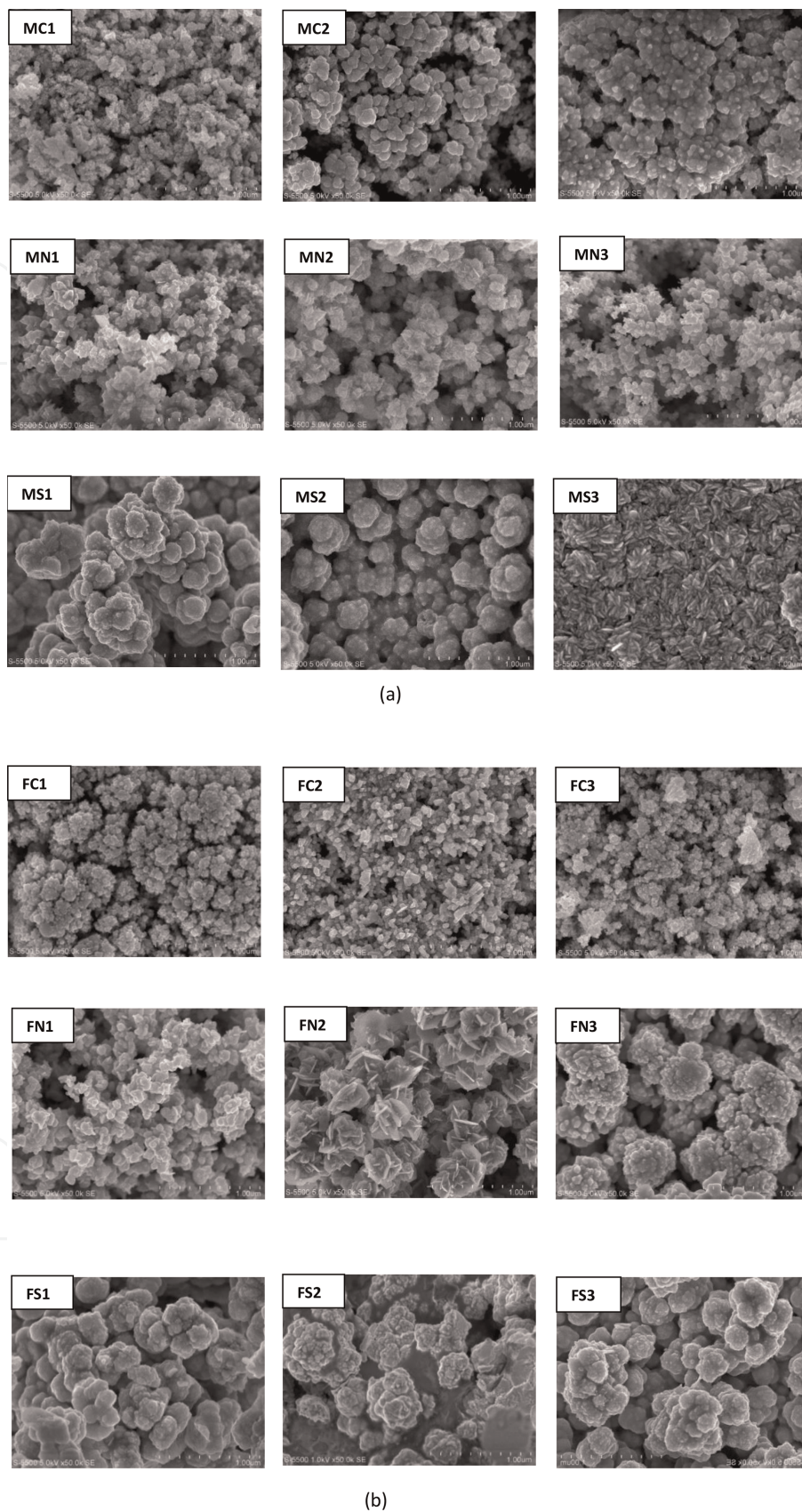


Figure 2. Micrographs of CIGS films, fabricated using Mo (M) and FTO (F) as substrates, various types of salts (chlorides (C), nitrates (N), or sulfates (S)) using sulfate salts at overpotentials of -1.0 V (1), -0.9 V (2), or -0.8 V (3).

3D instantaneous nucleation

$$\left(\frac{i}{i_{max}}\right)^2 = \left(\frac{1.9542}{\frac{t}{t_{max}}}\right) \times \left[1 - \exp\left(-1.2564\left(\frac{t}{t_{max}}\right)\right)\right]^2 \quad (5)$$

Figure 3 shows the potentiostat current-time plots obtained during the electrodeposition of CIGSe films.

This behavior is associated with an increase in the electroactive area and the stabilization and growth of new nuclei; subsequently, the slow decay of the current observer indicates a mass transfer-controlled process. The transients show the characteristic behavior of diffusion-controlled three-dimensional (3D) nucleation processes [24]. **Figure 3** shows the transients of CIGSe film samples on Mo substrates (**Figure 3(a–c)**) at three different applied overpotentials. **Figure 3(d–f)** shows CIGS films on FTO substrates and the three overpotentials used. Each figure shows the plots obtained by Eqs. (4) and (5), where the rapid and progressive 3D theoretical growths can be seen. It observed that for all samples, the values obtained with these equations show a behavior very close to the 3D-instantaneous change, which is favored to a greater extent in FTO substrates than in molybdenum/glass substrates. F. Liu et al. report the same type of nucleation and growth of CIGS films as presented in this work, using only an electrolytic bath of chloride salts [25]. According to our results, using electrolyte baths other than chlorides produces fast 3D growth.

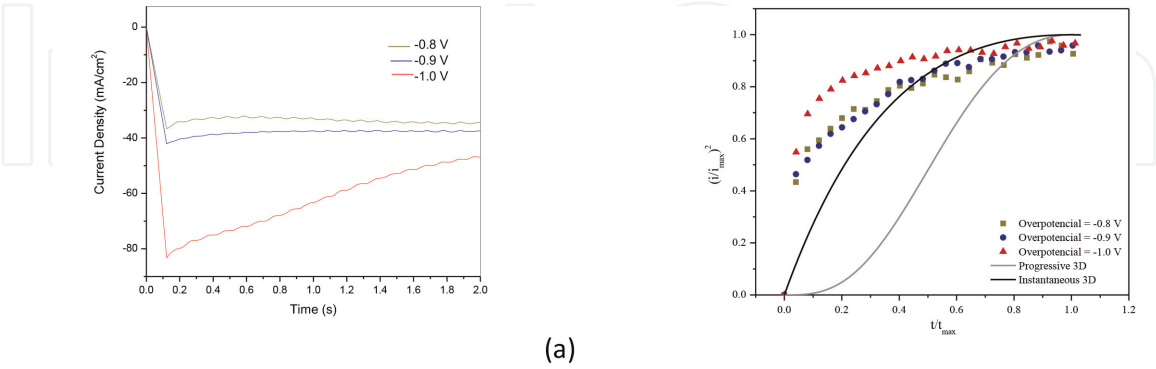
3.5 Optical properties

Table 5 shows the values obtained for the received bandwidth from the plots of $(F(R_{\infty}) \cdot h\nu)^2$ versus $h\nu$ for the CIGS films prepared on molybdenum (Mo) and FTO. (Where $(F(R_{\infty}) \cdot h\nu)^2$ is Kubelka-Munk function and $h\nu$ is the photon energy. As can be seen, the colored film on FTO has slightly higher bandwidth values than those deposited on Mo. These values are higher since the overpotential is higher for the films deposited on Mo and using chloride and sulfate electrolytic baths, but this is not the case for the nitrate ones. The results show that the value of the band gap in some films reported in the literature is about 1.14 eV, which suffers variations depending on the synthesis method; when comparing this value with those reported in **Table 5**, the values in this table are close.

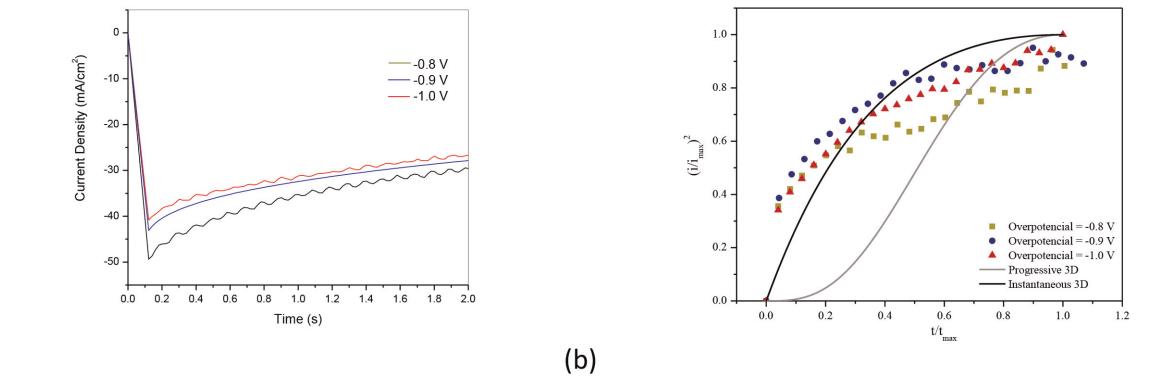
3.6 Electrochemical evaluation

Figure 4(a) shows a potential reduction peak probably due to gallium deposition, at -0.726 V vs. Ag/AgCl potential, at a sweep speed of 5 mV/s, since the elements of the precursor salts of copper chloride, indium chloride, and lithium chloride are not deposited. On the other hand, at the same sweep speed, an anodic potential is seen at approximately -0.350 V vs. Ag/AgCl due to gallium's oxidation. Furthermore, a potential crossover shows at approximately -0.360 V due to the formation of a deposit on the Mo electrode surface, possibly gallium. At the rates of 10 mV/s and 20 mV/s, no anodic or cathodic potential peaks are observed, so, likely, the Mo electrode is not stable in the presence of the chlorides coming from the precursor salts at these two sweep rates in an interval of -0.350 to -1.0 V vs. Ag/AgCl a pseudocapacitive zone.

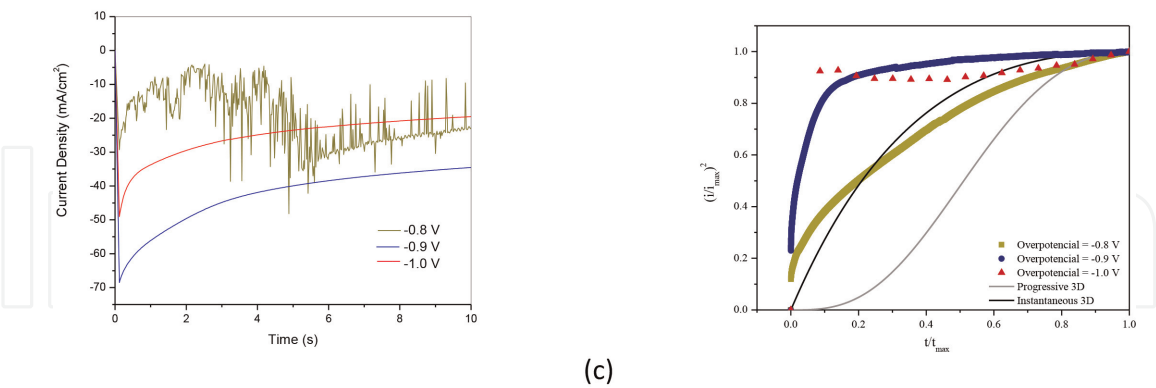
In **Figure 4c**, two consecutive potential peaks had been observed at approximately -0.002 and -0.05 V vs. Ag/AgCl, respectively, which probably attributed to Cu reduction on the Mo substrate at sweep speeds of 10 and 20 mV/s. An anodic potential peak appears at approximately 0.35 V and 0.75 V vs. Ag/AgCl, probably due to the oxidation of the Cu film formed. However, the pH is acidic, it is very likely that Ga,



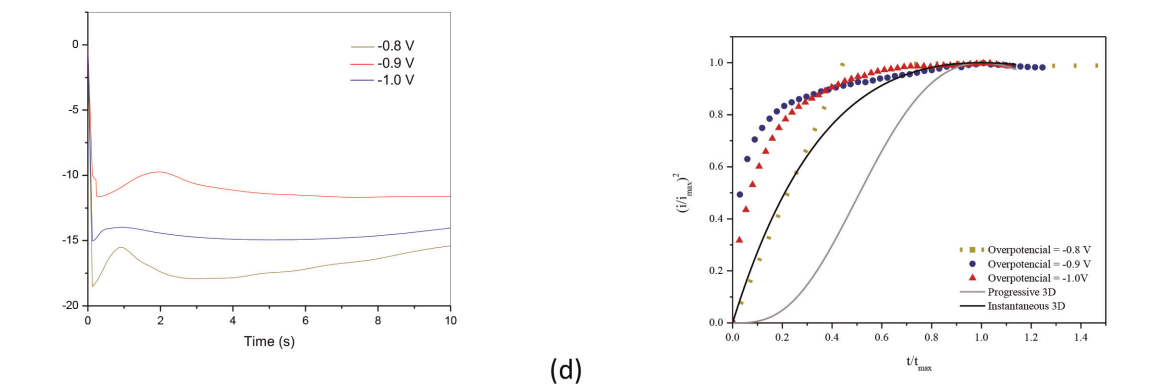
(a)



(b)



(c)



(d)

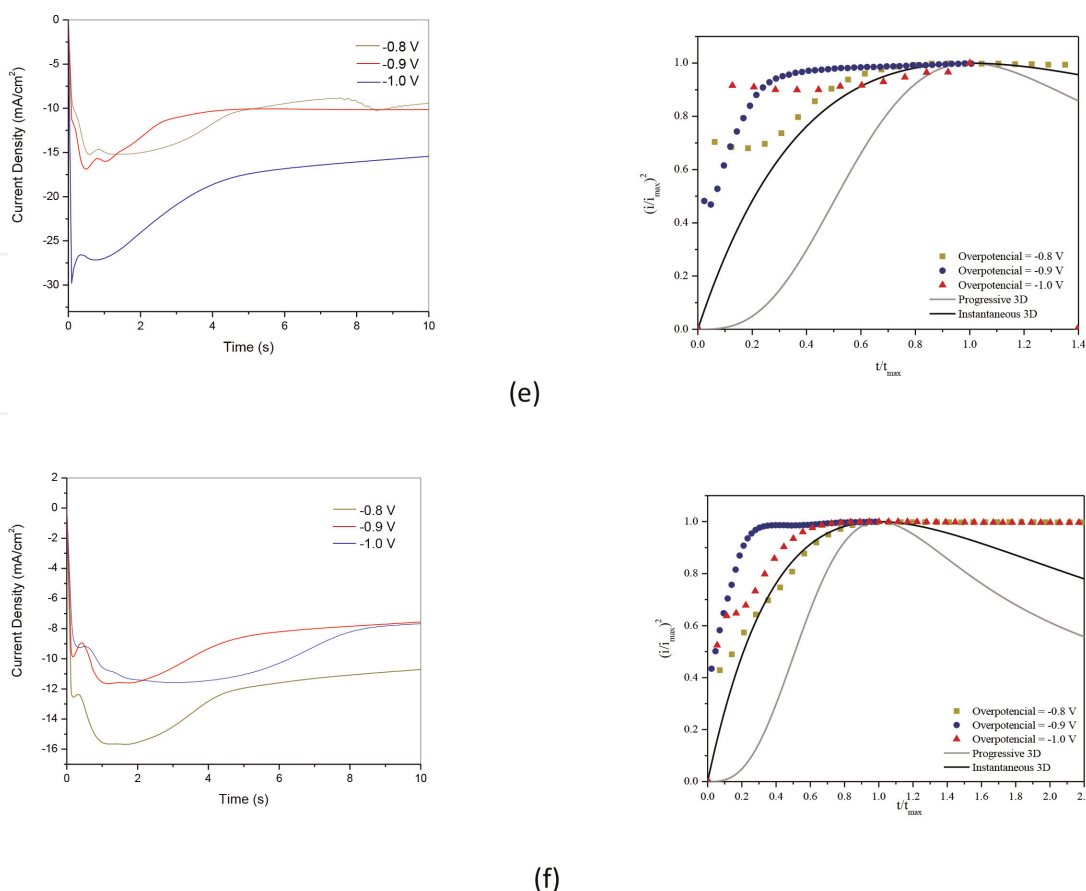


Figure 3. (a), (b), (c) correspond to CIGS time-current transients using molybdenum/glass as substrate and chloride, nitrate, and sulfate salts, respectively. (d), (e), (f) correspond to the time-current transients of CIGS using FTO as substrate and chloride, nitrate, and sulfate salts, respectively.

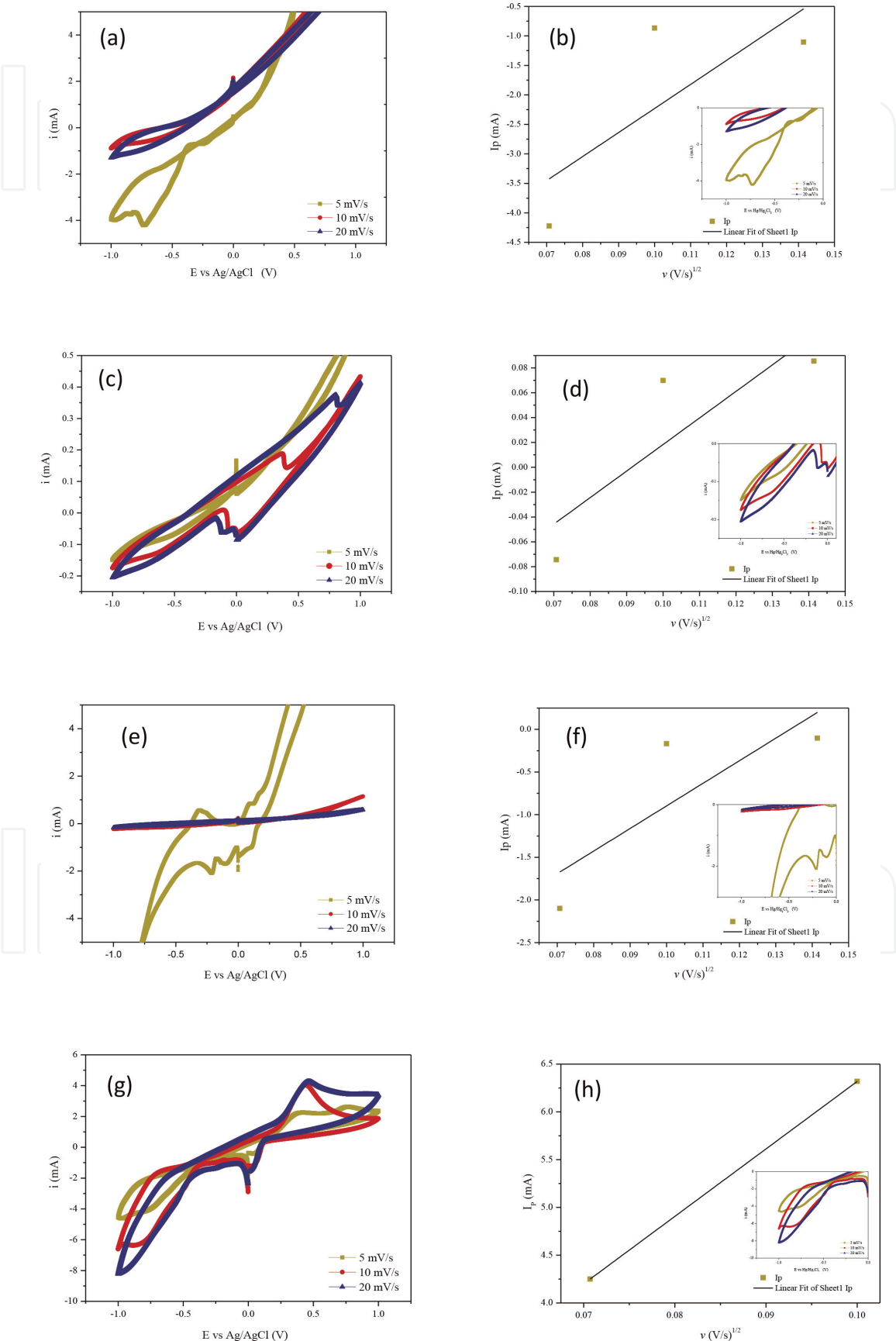
Sample	Band gap value (eV)	Sample	Band gap value
MC1	1.27	FC1	1.02
MC2	1.32	FC2	1.42
MC3	1.47	FC3	1.34
MN1	1.24	FN1	1.33
MN2	1.30	FN2	1.27
MN3	1.32	FN3	1.34
MS1	1.24	FS1	1.28
MS2	1.17	FS2	1.26
MS3	1.09	FS3	1.32

Table 5. Bandwidth values for the CIGS films made with the electrolytic baths had shown in Table 1.

In, and Li hydroxides of the precursor salts are starting on the electrode surface, based on Duchatelet A., Sidali T., et al. (2013). Consequently, this process does not allow these elements to deposit on the electrode. On the other hand, at the rate of 5 mV/s, no potential peaks are present.

Figure 4(e) shows three potential peaks associated with the reduction processes of the probable Cu, In, and Ga elements, at potentials of 0.012, -0.096 , and -0.205 V

vs. Ag/AgCl, respectively, at the rate of 5 mV/s, and at this same rate an anodic peak is present due to an oxidation process at approximately -0.307 V vs. Ag/AgCl. However, at the velocities of 10 and 20 mV/s, neither cathode nor anodic peaks are



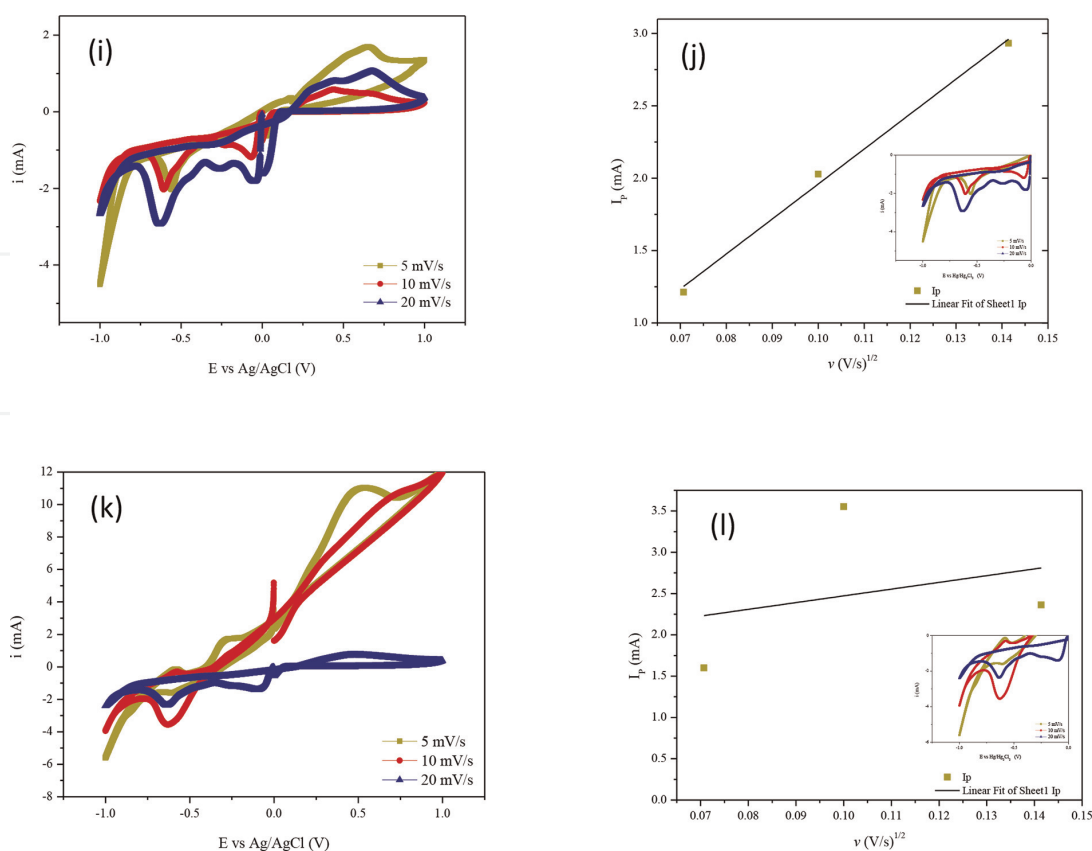


Figure 4. Plots of the CIGS films deposited on molybdenum (a, c, e) or FTO (g, i, k), using chloride, nitrate, and sulfate salts, respectively, at overpotentials of -1.0 V (red), -0.9 V (wine), and -0.8 V (brown) each. (b, d, f, h, j, l) show the graphs between the maximum current and the square root of the scanning speed of each of the sales respectively.

observed; this is probably because the deposited Mo film was unstable in the presence of sulfates.

Figure 4(g) shows a potential peak corresponding to a reduction process around -0.003 V vs. Ag/AgCl, probably due to Cu reduction. Likewise, an oxidation process at about 0.456 V vs. Ag/AgCl is possibly due to Cu. These processes appear at all three sweep rates 5, 10, and 20 mV/s, which means that the FTO electrode surface is stable in the presence of chlorides of the precursor salts.

Figure 4(i) shows three potential peaks corresponding to the reduction around -0.055 , -0.254 , and -0.600 V vs. Ag/AgCl, most probably deposited Cu, Ga, and In, respectively, and three oxidation processes observed at approximately 0.166 , 0.432 , and 0.677 V vs. Ag/AgCl, attributed to Cu, Ga, and In elements. These processes appear at the three scan rates of 5, 10, and 20 mV/s, which means that the FTO electrode surface is more stable than Mo in the presence of nitrates from the precursor salts.

Figure 4(k) shows two potential peaks mainly corresponding to reduction at about -0.083 and -0.644 V vs. Ag/AgCl, most probably deposited Cu, Ga, respectively, and two oxidation processes observed at about -0.590 and 0.542 V vs. Ag/AgCl, attributed to Cu, Ga elements. These processes appear at all three sweep rates, 5, 10, and 20 mV/s, which means that the FTO electrode surface is less stable in the presence of sulfates than in nitrates.

Figure 4 show the plots between the peak current and the square root of the scan rate of each of the sales, respectively, which generally follow a straight-line trajectory confirming that the electrodeposition process is diffusion controlled and irreversible [26]. Furthermore, this process had shown in films deposited on the FTO substrate (h, j, l).

4. Conclusions

The results conclude that the CIGSe films fabricated using chloride baths and employing Mo and FTO as a substrate have values similar to the ideal Ga/(In+Ga) ratio of 0.3. However, when using nitrate and sulfate-based baths, this ratio has values close to perfect equilibrium only for samples MN1 and MN2. The rest of the pieces have low values. It indicates that chloride-based baths favor incorporating Ga into the film to form an ideal relationship with the composition. The analysis performed by X-ray diffraction found that the main phase corresponds to $\text{CuGa}_{0.3}\text{In}_{0.7}\text{Se}_2$ (PDF #35-1102). Whose principal diffraction planes are (112), (220), and (116), which have been identified in all the elaborated samples, independently of the type of electrolytic bath used or the type of substrate. It is important to note that all diffractograms do not show adequate polycrystallinity, which attribute to the kind of growth. The growth of the CIGS films is cauliflower type for all samples, observing an increase in size for an applied deposition voltage, that is, lower using chlorides to higher using sulfates. According to the models, the nucleation process of the fabricated films is instantaneous with 3D growth, which is more noticeable when FTO had used as substrate. When Mo substrate uses, a smaller band gap of CIGS films is getting; these values increase when the applied over potential also increases when chloride and sulfate salts have used. According to the graphs of maximum peak current versus the square root of the sweep speed for each metal salt used, a linear trend with a positive slope observes; that is, there is a directly proportional correlation between these two parameters, according to the model of the current equation and the sweep speed for cyclic voltammetry.

Acknowledgements

This work was supported through the PAPIIT-IN111320 project and the CONACyT Postdoc grant. We also thank Maria Luisa Ramón Garcia for XRD measurements, Rogelio Moran Elvira for SEM measurements, and José Campos Álvarez for EDS assistance.

Author details


Arelis Ledesma Juárez¹, Alejandro Altamirano Gutiérrez² and Arturo Fernández Madrigal^{1*}

¹ Instituto de Energías Renovables, Universidad Nacional Autónoma de México, Morelos, México

² Centro Universitario de Tonalá, Universidad de Guadalajara, Jalisco, México

*Address all correspondence to: afm@ier.unam.mx

IntechOpen

© 2023 The Author(s). Licensee IntechOpen. This chapter is distributed under the terms of the Creative Commons Attribution License (<http://creativecommons.org/licenses/by/3.0>), which permits unrestricted use, distribution, and reproduction in any medium, provided the original work is properly cited. 

References

- [1] Regmil G, Ashok A, Chawla P, Semalti P, Velumani S, Shailesh N, et al. Perspectives of chalcopyrite-based CIGSe thin-film solar cell: A review. *Journal of Materials Science: Materials in Electronics*. 2020;**31**:7286-7314. DOI: 10.1007/s10854-020-03338-2
- [2] Green MA, Dunlop ED, Levi DH, Ebinger H, Yoshita J, Ho-Baillie AW, et al. Solar cell efficiency tables (version 54). *Progress in Photovoltaics*. 2019;**27**: 565-575. DOI: 10.1002/pip.3371
- [3] Nakamura M, Yamaguchi K, Kimoto Y, Yasaki Y, Kato T, Sugimoto H. Cd-free Cu(In, Ga)(Se, S)₂ thin-film solar cell with record efficiency of 23.35%. *IEEE Journal of Photovoltaics*. 2019;**9** (6):1863-1867. DOI: 10.1109/JPHOTOV.2019.2937218
- [4] Powalla M, Paetel S, Ahlswede E, Wuerz R, Wessendorf CD, Friedlmeier TM. Thin-film solar cells exceeding 22% solar cell efficiency: An overview on CdTe-, Cu(In, Ga)Se₂-, and perovskite-based materials. *Applied Physics Reviews*. 2018;**5**:041602. DOI: 10.1063/1.5061809
- [5] Pandey RK, Sahu SN, Chandra S. *Handbook of Semiconductor Electrodeposition*. New York, Basel, Hong Kong: Marcel Dekker, Inc.; 1996
- [6] Lincot D, Guillemoles JF, Taunier S, Guimard D, Sicx-Kurdi J, Chaumont A, et al. Chalcopyrite thin film solar cells by electrodeposition. *Solar Energy*. 2004;**77** (6):725-737. DOI: 10.1016/j.solener.2004.05.024
- [7] Lincot D. Electrodeposition of semiconductors. *Thin Solid Films*. 2005; **487**(1-2):40-48. DOI: 10.1016/j.tsf.2005.01.032
- [8] Johnson DR. Microstructure of electrodeposited CdS/CdTe cells. *Thin Solid Films*. 2000;**361-362**:321-326. DOI: 10.1016/S0040-6090(99)00779-8
- [9] Chirilă A, Reinhard P, Pianezzi F, Bloesch P, Uhl AR, Fella C, et al. Potassium-induced surface modification of Cu(In, Ga)Se₂ thin films for high-efficiency solar cells. *Nature Materials*. 2013;**12**:1107. DOI: 10.1038/nmat3789
- [10] Reinhard P, Bissig B, Pianezzi F, Avancini E, Hagendorfer H, Keller D, et al. Features of KF and NaF postdeposition treatments of Cu(In, Ga)Se₂ absorbers for high-efficiency thin film solar cells. *Chemistry of Materials*. 2015;**27**:5755-5764. DOI: 10.1021/acs.chemmater.5b02335
- [11] Friedlmeier TM, Jackson P, Bauer A, Hariskos D, Kiowski O, Wuerz R, et al. Improved photocurrent in Cu(In, Ga)Se₂ solar cells: From 20.8% to 21.7% efficiency with CdS buffer and 21.0% Cd-free. *IEEE Journal of Photovoltaics*. 2015;**5**:1487-1491. DOI: 10.1109/JPHOTOV.2015.2458039
- [12] Liu J, Liu F, Lai Y, Zhang Z, Li J, Liu Y. Effects of sodium sulfamate on electrodeposition of Cu(In, Ga)Se₂ thin film. *Journal of Electroanalytical Chemistry*. 2011;**1**(65):191-196. DOI: 10.1016/j.jelechem.2010.10.021
- [13] Muthuraj JJJ, Rasmussen DH, Suni II. Electrodeposition of CuGaSe₂ from thiocyanate-containing electrolytes. *Journal of the Electrochemical Society*. 2011;**158**:D54. DOI: 10.1149/1.3519997
- [14] Stratieva N, Tzvetkova E, Ganchev M, Kochev K, Tomov I. Structural and optical properties of electrodeposited CuInSe₂ layers. *Solar Energy Materials*

& Solar Cells. 1997;**45**:87-96. DOI: 10.1016/S0927-0248(96) 00070-0

[15] Aksu S, Wang J, Basol BM. Electrodeposition of In–Se and Ga–Se thin films to prepare CIGS solar cells. *Electrochem. Solid State Lett.* 2009;**12**: D33. DOI: 10.1149/1.3079481

[16] Morales AE, Mora ES, Pal U. Use of diffuse reflectance spectroscopy for optical characterization of un-supported nanostructures. *Revista Mexicana de Fisica.* 2007;**53**(5):18-22

[17] Abdullahi SS, Güner S, Koseoglu Y, Musa IM, Adamuy BI, Abdulhamid MI. Simple method for the Determination of the band gap of a Nanopowdered sample Using Kubelka Munk theory. *Journal of the Nigerian Association of Mathematical Physics.* 2016;**35**:241-246

[18] Farooq L, Alraeesi A, Zahmi SA. A review on the electrodeposition of CIGS thin-film solar cells. *IEOM Society International.* 2019;**26**(28):158-185. Corpus ID: 223560420

[19] Eberspacher C, Fredric C, Pauls KS. Thin-film CIS, alloy PV materials, fabricated using non-vacuum, particles-based techniques. *Thin Solid Films.* 2001;**387**:18-22. DOI: 10.1016/S0040-6090(00)01729-6

[20] Lee H, Yoon H, Ji H, Lee D, Lee J, Yun J, et al. Fabrication of CIGS films by electrodeposition method for photovoltaic cells. *Journal of Electronic Materials.* 2012;**41**(12):3375-3381. DOI: 10.1007/ s11664-012-2252-x

[21] Holzwarth U, Gibson N. The Scherrer equation versus the Debye-Scherrer equation. *Nature Nanotechnology.* 2011;**6**:534. DOI: 10.1038/nnano.2011.145

[22] Saïdia H, Ben Alayaa C, Boujmila MF, Durand B, Lazzari JL, Bouaïcha M. Physical properties of electrodeposited CIGS films on crystalline silicon: Application for photovoltaic hetero-junction. *Current Applied Physics.* 2020; **20**:29-36. DOI: 10.1016/j.cap.2019.09.015

[23] Pourbaix M. *Atlas of Electrochemical Equilibria in - Aqueous Solutions.* Houston, Texas: National Association of Corrosion Engineers; 1974. p. 77084

[24] Scharifker B, Hills G. Theoretical and experimental studies of multiple nucleation. *Electrochimica Acta.* 1983; **28**:879-889

[25] Gupta A, Srivastava C. Nucleation and growth mechanism of tin electrodeposition on graphene oxide: A kinetic, thermodynamic and microscopic study. *Journal of Electroanalytical Chemistry.* 2020;**861**:113964 (1-8). DOI: 10.1016/j.jelechem.2020.113964

[26] Liu F, Huang C, Lai Y, Zhang Z, Li J, Liu Y. Preparation of Cu (In, Ga) Se₂ thin films by pulse electrodeposition. *Journal of Alloys and Compounds.* 2011; **509**:L129-L133. DOI: 10.1016/j.jallcom.2010.12.031